IMPLEMENTATION OF CORNER POINT MESH INTO A PARALLEL, FULLY IMPLICIT, EQUATION OF STATE COMPOSITIONAL RESERVOIR SIMULATOR

Francisco Marcondes*
Mechanical Engineering Department, Federal University of Ceará, Campus do Pici, MB: 12.144 – 60455-760–Fortaleza–CE, Brazil
marconde@dem.ufc.br

Choongyong Han
Center for Petroleum and Geosystems Engineering, University of Texas at Austin, Austin, TX 78712-0228
cyhan@mail.utexas.edu

Kamy Sepehrnoori
Petroleum and Geosystems Engineering Department, University of Texas at Austin, Austin, TX 78712-0228
kamys@mail.utexas.edu

* Now on leave at the Center for Petroleum and Geosystems Engineering, University of Texas at Austin, Austin, TX 78712-0228

Abstract. *Design and application of an enhanced oil recovery (EOR) process is one of the important tasks performed by reservoir engineers to increase oil recovery from reservoirs after water flooding. A compositional reservoir simulator can be used to facilitate the design of a particular EOR process and also aid prediction of the ultimate oil recovery. A three-dimensional, fully implicit, multiphase/multi-component, parallel reservoir simulator called GPAS capable of simulating a variety of enhanced oil recovery processes has been developed at the Center for Petroleum and Geosystems Engineering at the University of Texas to aid reservoir engineers with EOR simulations. The simulator consists of two main sections: Framework and EOScomp. Framework handles the input/output as well as parallel processing tasks. EOScomp performs the computations for the solutions of the equations arising from discretization of governing partial differential equations which model the movements of fluids in the reservoir. The simulator was developed using Cartesian grids, hence it did not have the capability of easily handling a reservoir with irregular boundaries and faults. The main focus of this paper is the implementation of corner point mesh into GPAS. In this paper, the formulation for the new implementation as well as the results using corner mesh in conjunction with reservoir simulation case studies are presented. Also, the results of simulation studies using single and multiprocessors are presented in this paper.*

Keywords*: Compositional Model, Corner Point Mesh, Fully Implicit Procedure, Parallel Computation, Finite Volume Method.*

1. Introduction

Enhanced oil recovery (EOR) is of vital importance for oil production since a large amount of hydrocarbons is left in the reservoirs after the secondary recovery process. Compositional reservoir simulators are used to aid the design and implementation of EOR processes. A compositional reservoir simulator called GPAS (General Purpose Adaptive Simulator) was developed, at the Center for Petroleum and Geosystems, for simulation of EOR processes. GPAS is a three-dimensional, fully implicit, multiphase/multi-component, parallel reservoir simulator that can handle simulation of several enhanced oil recovery processes. In parallel mode, message passing between the processors is performed using MPI (Snir et al., 1986). GPAS is divided into two main modules: Framework and EOScomp. Framework is responsible for input/output, domain decomposition, and memory allocation, while EOScomp handles the computations for flash calculation and solution of nonlinear equations arising from discretization of the governing equations. Details of EOScomp and Framework modules can be found in Wang et al. (1997) and Parashar et al. (1997), respectively. The simulator was developed using Cartesian mesh. Although this kind of mesh is very easy to generate, it cannot handle several features of the reservoir such as irregular boundaries and faults. One possible option to overcome this restriction is the use of boundary fitted coordinates (Thompson et al., 1985, and Maliska, 2004). This kind of mesh is named structured corner point mesh in petroleum reservoir simulation, (Edwards, 1998). Therefore, the main focus of this paper is to implement structured corner point mesh into GPAS. In the following sections, the new formulation using corner point mesh and the results of simulation case studies using single and multiprocessors are presented.

2. Physical model

Isothermal multi-component multiphase fluid flow in a porous media can be described using three types of equations: partial differential component-material balance equation, phase equilibrium equation, and equation constraining phase saturations and component concentrations (Wang et al., 1997).

The material balance equation for i-th component assuming diagonal permeability tensor can be written in a Cartesian system as

$$\frac{\partial(\phi N_i)}{\partial t}-\frac{\partial}{\partial x}\left(\sum_{j=1}^{np}\xi_j\, x_{ij}\,\lambda_{rj}K_{xx}\frac{\partial\Phi_j}{\partial x}\right)-\frac{\partial}{\partial y}\left(\sum_{j=1}^{np}\xi_j\, x_{ij}\,\lambda_{rj}K_{yy}\frac{\partial\Phi_j}{\partial y}\right)-\frac{\partial}{\partial z}\left(\sum_{j=1}^{np}\xi_j\, x_{ij}\,\lambda_{rj}K_{zz}\frac{\partial\Phi_j}{\partial z}\right)-q_i=0\,, \tag{1}$$

where n_p is the number of phases present in the reservoir, ϕ is the porosity, N_i is the mole of i-th component per unit of pore volume, ξ_j and λ_{rj} are the molar density and relative mobility of j-th phase respectively, and K_{xx}, K_{yy}, and K_{zz} are the diagonal components of absolute permeability tensor. Φ_j is the potential of j-th phase and is given by

$$\Phi_j=P_j-\gamma_j Z \tag{2}$$

In Eq. (2), P_j denotes the pressure of j-th phase and Z is depth which is positive in downward direction.

The first partial derivative of the total Gibbs free energy with respect to the independent variables gives equality of component fugacities among all phases,

$$f_i=f_i^j-f_i^r=0\ \ ;\ \ i=1,....,n_c\ \ \ ;\ \ j=2,.....,n_p \tag{3}$$

In Eq. (3), $f_i^j=\ln\left(x_{ij}\,\phi_{ij}\right)$, where x_{ij} is the molar fraction of i-th component in j-th phase, ϕ_{ij} is the fugacity coefficient of component i in j-th phase, r denotes the reference phase, and n_c is the number of components excluding water. The restriction of molar fraction is used to obtain the solution of Eq. (3),

$$\sum_{i=1}^{n_c}x_{ij}-1=0\,,\ (j=2,..,n_p)\ ;\quad \sum_{i=1}^{n_c}\frac{z_i\,(K_i-1)}{1+\nu\,(K_i-1)}=0\,, \tag{4}$$

where z_i is the overall molar fraction of i-th component, K_i is the equilibrium ratio for the i-th component, and ν is mole fraction of gas phase in absence of water. The closure equations come from volume constraint. The total pore volume of each cell must be filled with fluid. This constraint gives rise to

$$V_b\sum_{i=1}^{n_c+1}(\phi N_i)\sum_{j=1}^{n_p}L_j\,\bar{v}_j-V_p=0\,, \tag{5}$$

where V_b is the bulk volume, V_p is pore volume, and $\bar{v}_j$ is the molar volume of the j-th phase. In GPAS the unknown primary variables are water pressure P_w, N_1,..,N_{nc}, $\ln K_1$,.., $\ln K_{nc.}$

2. Transformed and approximate equations

In the approach adopted in this work the equations are transformed from the Cartesian system to a computational domain. Then, the transformed equations are integrated in the regular system, as described in Maliska (2004). The only equation that needs to be modified is the material balance equation of each component (Eq. (1)). Figure 1a shows the physical and computational domains. Equation (1) can be written in a boundary fitted coordinate system using the following transformation:

$$\xi=\xi(x,y,z)\ \ ;\ \ \eta=\eta(x,y,z)\ ;\ \gamma=\gamma(x,y,z) \tag{6}$$

The final transformed equation for the i-th component is given by

$$\frac{\partial}{\partial t}\left(\frac{\phi N_i}{J_t}\right)-\frac{\partial}{\partial \xi}\left(\sum_{j=1}^{np} D_{11ij}\frac{\partial \Phi_j}{\partial \xi}\right)-\frac{\partial}{\partial \xi}\left(\sum_{j=1}^{np} D_{12ij}\frac{\partial \Phi_j}{\partial \eta}\right)-\frac{\partial}{\partial \xi}\left(\sum_{j=1}^{np} D_{13ij}\frac{\partial \Phi_j}{\partial \gamma}\right)-\frac{\partial}{\partial \eta}\left(\sum_{j=1}^{np} D_{21ij}\frac{\partial \Phi_j}{\partial \xi}\right)-$$
$$\frac{\partial}{\partial \eta}\left(\sum_{j=1}^{np} D_{22ij}\frac{\partial \Phi_j}{\partial \eta}\right)-\frac{\partial}{\partial \eta}\left(\sum_{j=1}^{np} D_{23ij}\frac{\partial \Phi_j}{\partial \gamma}\right)-\frac{\partial}{\partial \gamma}\left(\sum_{j=1}^{np} D_{31ij}\frac{\partial \Phi_j}{\partial \xi}\right)-\frac{\partial}{\partial \gamma}\left(\sum_{j=1}^{np} D_{32ij}\frac{\partial \Phi_j}{\partial \eta}\right)-\frac{\partial}{\partial \gamma}\left(\sum_{j=1}^{np} D_{33ij}\frac{\partial \Phi_j}{\partial \gamma}\right)-\frac{q_i}{J_t}=0 \quad (7)$$

where J_t is the jacobian of the transformation and the tensor D involves fluid, reservoir, and geometric information. It is worthwhile to mention that although D is symmetric, it has nine elements instead of 3 compared to original diagonal permeability tensor given in Eq. (1).

Integrating Eq. (7) in control volume of Fig. 1b and time results in the following approximate equation:

$$\left(\frac{\phi N_i}{J_t}\right)_P^{n+1}\frac{\Delta V}{\Delta t}-\left(\frac{\phi N_i}{J_t}\right)_P^{n}\frac{\Delta V}{\Delta t}-\sum_{j=1}^{np} D_{11ij,e}^{n+1}\frac{\partial \Phi_j}{\partial \xi}\bigg|_e^{n+1}\Delta\eta\Delta\gamma+\sum_{j=1}^{np} D_{11ij,w}^{n+1}\frac{\partial \Phi_j}{\partial \xi}\bigg|_w^{n+1}\Delta\eta\Delta\gamma-\sum_{j=1}^{np} D_{12ij,e}^{n+1}\frac{\partial \Phi_j}{\partial \eta}\bigg|_e^{n}\Delta\eta\Delta\gamma+ \quad (8)$$
$$\sum_{j=1}^{np} D_{12ij,w}^{n+1}\frac{\partial \Phi_j}{\partial \eta}\bigg|_w^{n}\Delta\eta\Delta\gamma-\sum_{j=1}^{np} D_{13ij,e}^{n+1}\frac{\partial \Phi_j}{\partial \gamma}\bigg|_e^{n}\Delta\eta\Delta\gamma+\sum_{j=1}^{np} D_{13ij,w}^{n+1}\frac{\partial \Phi_j}{\partial \gamma}\bigg|_w^{n}\Delta\eta\Delta\gamma-\sum_{j=1}^{np} D_{21ij,n}^{n+1}\frac{\partial \Phi_j}{\partial \xi}\bigg|_n^{n}\Delta\xi\Delta\gamma+\sum_{j=1}^{np} D_{21ij,s}^{n+1}\frac{\partial \Phi_j}{\partial \xi}\bigg|_s^{n}\Delta\xi\Delta\gamma$$
$$-\sum_{j=1}^{np} D_{22ij,n}^{n+1}\frac{\partial \Phi_j}{\partial \eta}\bigg|_n^{n+1}\Delta\xi\Delta\gamma+\sum_{j=1}^{np} D_{22ij,s}^{n+1}\frac{\partial \Phi_j}{\partial \eta}\bigg|_s^{n+1}\Delta\xi\Delta\gamma-\sum_{j=1}^{np} D_{23ij,n}^{n+1}\frac{\partial \Phi_j}{\partial \gamma}\bigg|_n^{n}\Delta\xi\Delta\gamma+\sum_{j=1}^{np} D_{23ij,s}^{n+1}\frac{\partial \Phi_j}{\partial \gamma}\bigg|_s^{n}\Delta\xi\Delta\gamma-$$
$$\sum_{j=1}^{np} D_{31ij,f}^{n+1}\frac{\partial \Phi_j}{\partial \xi}\bigg|_f^{n}\Delta\xi\Delta\eta+\sum_{j=1}^{np} D_{31ij,b}^{n+1}\frac{\partial \Phi_j}{\partial \xi}\bigg|_b^{n}\Delta\xi\Delta\eta-\sum_{j=1}^{np} D_{32ij,f}^{n+1}\frac{\partial \Phi_j}{\partial \eta}\bigg|_f^{n}\Delta\xi\Delta\eta+\sum_{j=1}^{np} D_{32ij,b}^{n+1}\frac{\partial \Phi_j}{\partial \eta}\bigg|_b^{n}\Delta\xi\Delta\eta-\sum_{j=1}^{np} D_{33ij,f}^{n+1}\frac{\partial \Phi_j}{\partial \gamma}\bigg|_f^{n+1}\Delta\xi\Delta\eta$$
$$+\sum_{j=1}^{np} D_{33ij,b}^{n+1}\frac{\partial \Phi_j}{\partial \gamma}\bigg|_b^{n+1}\Delta\xi\Delta\eta-\frac{q_{i,P}^{n+1}\Delta V}{J_{t,P}}=0$$

A semi-implicit procedure was used to solve the approximate equation. In order not to increase the non-zero diagonals in the coefficient matrix of the linear system of equations, the cross terms were included in the right hand side of the residual function. This procedure can reduce the convergence rate of the linear system if the mesh is highly distorted. However, it is worthwhile to mention that this procedure reproduces the exact mass flow rate along each interface of the control volume.

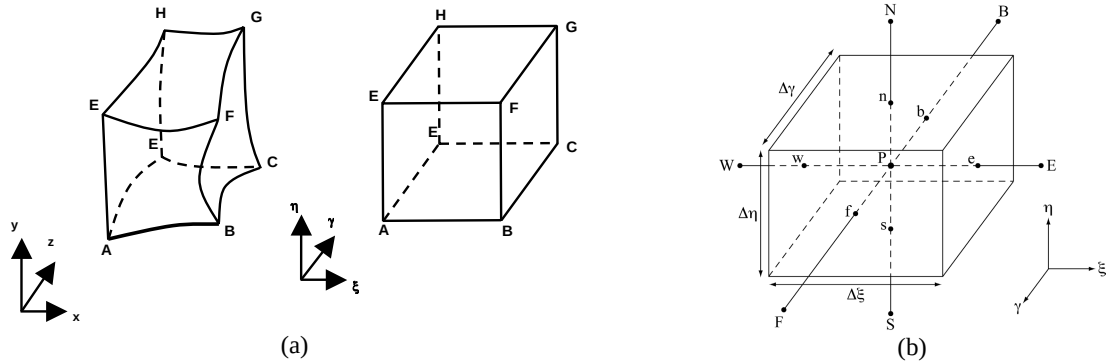

Figure 1. (a) Physical and computational domains (b) Control volume.

3. Results

Two cases were considered to validate the implementation of corner point mesh. Case 1 refers to the simulation of water injection into a quarter of five spot and the simultaneous flow of water, oil, and gas. This problem was solved using a uniform Cartesian mesh (16x16x10 using the original code) and a corner point mesh (16x16x10 using the modified code) as shown in Fig. 2. The fluid and reservoir properties are given in Tab. 1. The relative permeabilities are evaluated using the Stone II Model (Stone,1973). The curves used to evaluate these permeabilities are presented in Fig. 3. There is no reason to use a non-orthogonal mesh for this kind of reservoir that contains no geological fault or heterogeneities, but this case was used just to validate the results of the corner point mesh with the original GPAS using a Cartesian mesh. Since the results should be independent of the mesh used, it is expected to obtain close agreement

between the non-orthogonal and Cartesian meshes if the fluxes and geometric information are computed correctly. Figure 4 presents the water, oil, and gas production rates respectively for the quarter of five-spot simulation. As can be seen in Fig. 4, despite the large differences in the configurations of the mesh used in the simulations, the results obtained with regular Cartesian mesh and non-orthogonal mesh are in good agreement.

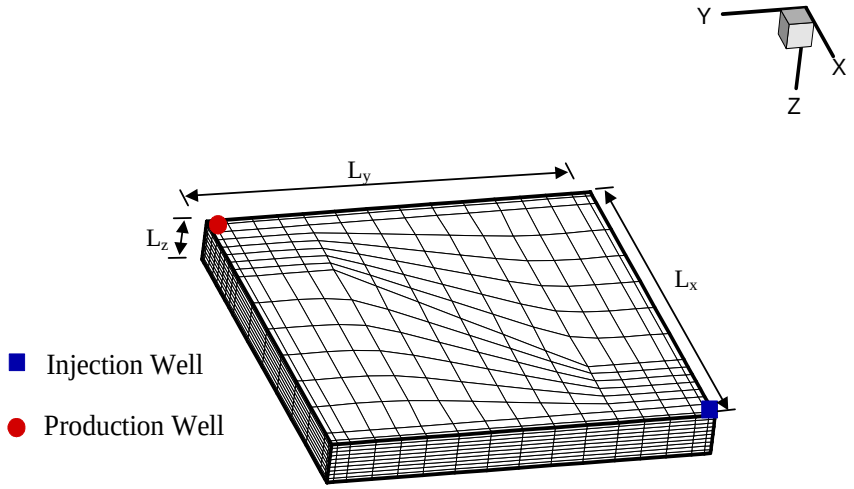

Figure 2. Non-orthogonal mesh for Case 1.

Table 1. Input data for Case 1.

Reservoir data	Initial conditions	Physical properties and well conditions
Reservoir dimension (L_x = L_y = 170.69 m, L_z = 30.48 m) Absolute permeability (K_{xx}= K_{yy} = K_{zz}) = $1.0x10^{-14}$ m^2 (10mD) Porosity = 0.350	Water saturation S_{wi} = 0.17 Reservoir pressure = 10.35 MPa (1500 psi) Overall fraction of hydrocarbon components (C1, C3, C6, C10, C15, C20) = 0.5, 0.03, 0.07, 0.2, 0.15, 0.05	Water viscosity = $1x10^{-3}$ Pa.s Water injection rate = 79.5 m^3/d Bottom hole pressure = 8.965 MPa (1300 psi)

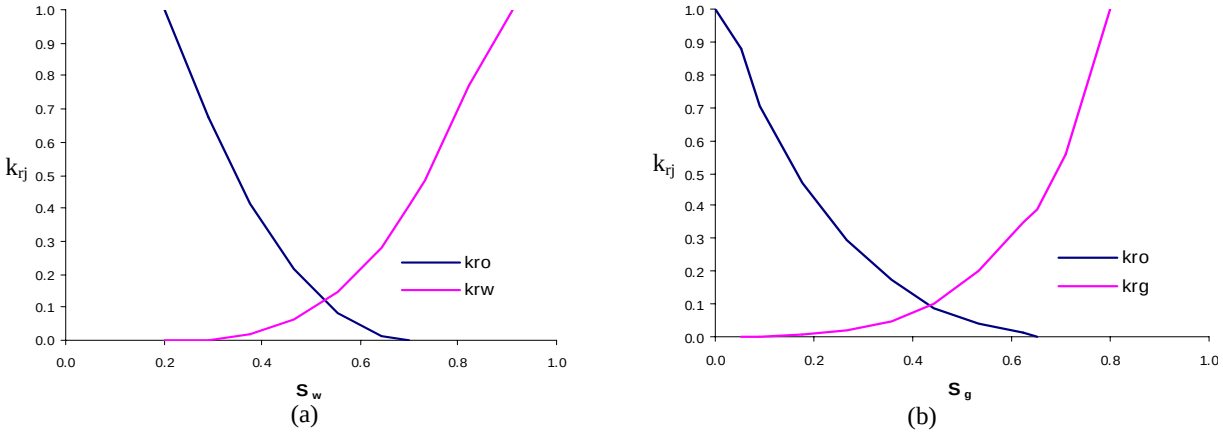

Figure 3. Relative permeability curves used in the Stone II model.

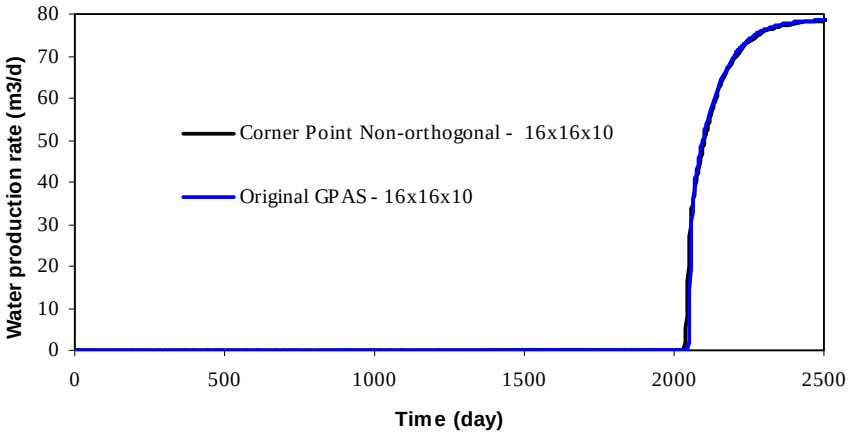

(a)

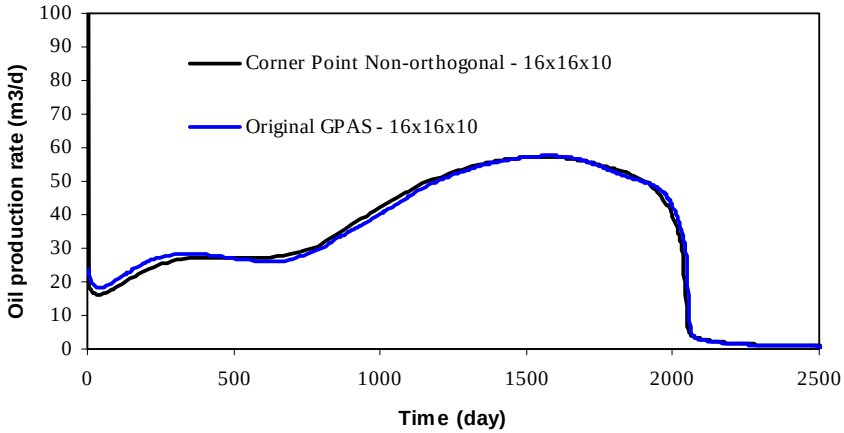

(b)

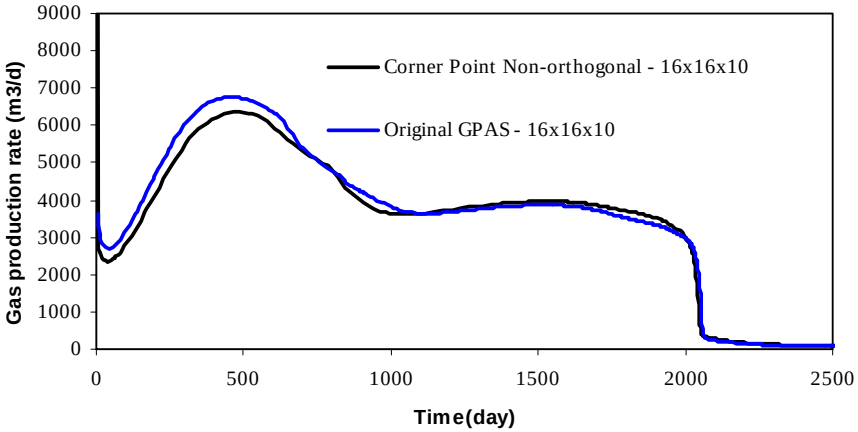

(c)

Figure 4. Results for Case 1 (a) Water production rate vs. time (b) Oil production rate vs. time (c) Gas production rate vs. time.

Case 2 presents simulation of a reservoir with eight wells (four injection and four production wells, see Fig. 5). Water is injected at constant rate through the injection wells. The input data for this case is presented in Tab. 2. The relative permeability curves shown in Fig. 3a were used for this case. This simulation was carried out using 45x24x4 gridblocks in conjunction with the corner point mesh implementation. A grid refinement study was also performed using the same case, but with 60x32x5 gridblocks. Both simulations were performed for 25,000 days. Figures 6a and 6b present the oil saturation field in 1012 and 20,000 days, respectively. From Fig. 6a, it is seen that water flows radially close to injection wells which is an expected behavior since each well is still injecting water in an isolated way. Figure 6b shows a situation in which most part of the reservoir is flooded by water after 20,000 days.

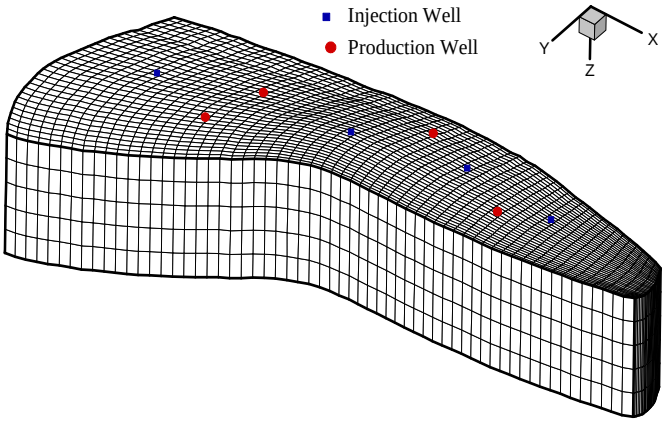

Figure 5. Non-orthogonal mesh for Case 2.

Table 2. Input data for Case 2.

Data of the reservoir	Initial conditions	Physical properties and well conditions
Absolute permeability (K_{xx}= K_{yy} = K_{zz}) = 1.0x10^{-13} m^2 (100mD) Thickness = 15.24 m Area = 3.4706x10^4 m^2 Porosity = 0.350	Water saturation S_{wi} = 0.17 Reservoir pressure = 10.35 MPa (1500 psi) Overall fraction of hydrocarbon components (C10, C15, C20) = 0.7, 0.2, 0.1	Water viscosity = 1x10^{-3} Pa.s Water injection rate = 954.0 m^3/d Bottom hole pressure = 8.965 MPa (1300 psi)

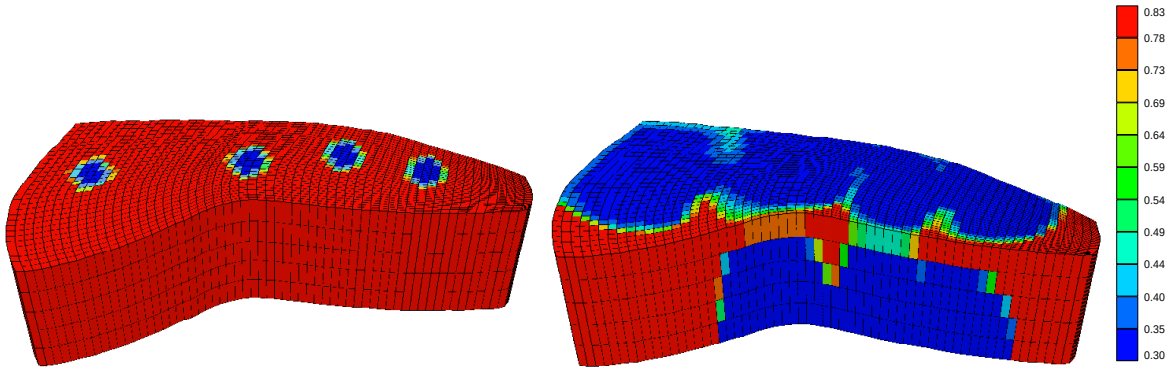

(a) (b)

Figure 6. Oil saturation field (a) 1,012 days (b) 20,000 days.

The simulation results for the grid refinement are presented in Fig. 7. For this case, only the production rates of water and oil are shown since this case corresponds to an undersaturated reservoir. As can be seen in Fig. 7, good agreements were obtained using both mesh configurations.

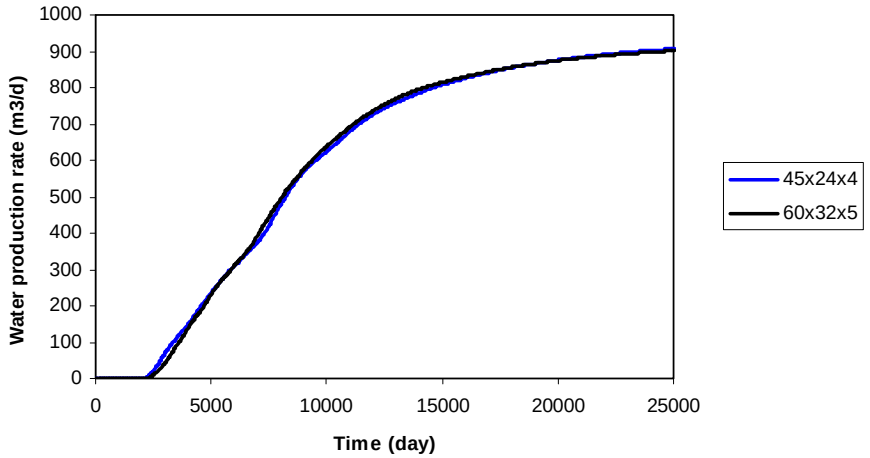

(a)

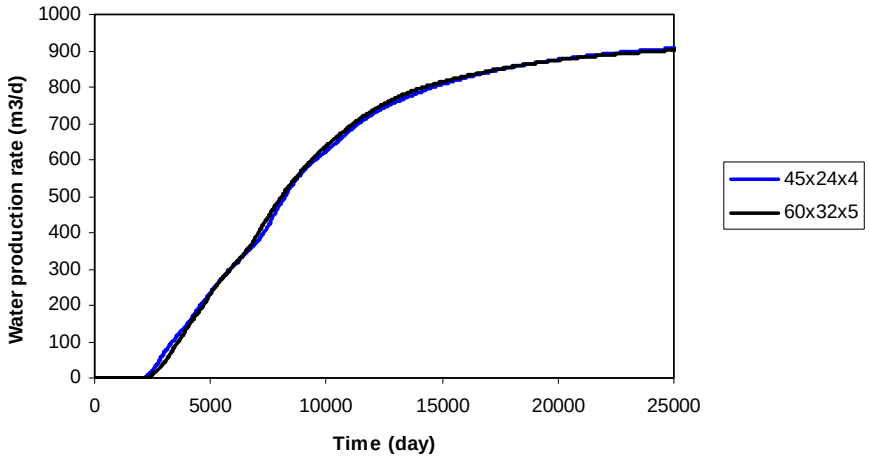

(b)

Figure 7. Results for Case 2 (a) Water production rate vs. time (b) Oil production rate vs. time.

In order to verify the efficiency of GPAS in parallel processing mode, simulation runs using Case 2 (the reservoir with four injection and four production wells) were performed. The simulations were carried out using a 60x32x5 gridblocks for 2000 days. In order to examine the speedup efficiency, simulation runs were performed using 1, 2, 4, 8, and 16 processors. The results for this study are presented in Fig. 8. As it can be seen in the figure, good speedups were obtained as the number of processors was varied from one to sixteen. All of the simulations were performed using a cluster of workstation with dual processors having the speed of 3.20 GHz, 2 GB memory, and Myrinet as switch. Comparison of GPAS with commercial simulators is underway and the results of this comparison will appear in our future publications.

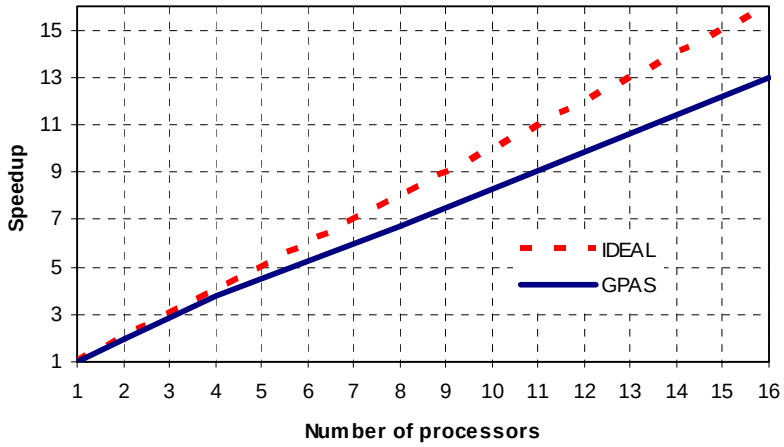

Figure 8. Parallel performance speedup for Case 2.

4. Conclusions

This work presented implementation of a corner point mesh into a fully implicit parallel compositional reservoir simulator called GPAS. The new implementation was verified by comparing the results generated using the simulator with the corner point mesh and the original Cartesian mesh. Good agreements were obtained using the two different approaches. Initial results using the simulator in parallel mode in conjunction with the corner point mesh displayed good speedup as larger number of processors was used for the simulations.

5. Acknowledgements

This work was conducted with the support of Reservoir Simulation Joint Industry Project, a consortium of operating and service companies at the Center for Petroleum and Geosystems Engineering at The University of Texas at Austin. Also, the first author would like to thank CAPES (Brazilian Educational Agency) for their financial support.

6. References

Edwards, M. G., 1998. Simulation with a Full Tensor Coefficient Velocity Field Recovered from a Diagonal Tensor Solution, *paper SPE 49073, SPE Annual Technical Conference and Exhibition*, New Orleans, USA, pp. 383-391.

Maliska, C. R., 2004. *Heat Transfer and Computational Fluid Mechanics*, Florianópolis, 2ª. Ed., Editora LTC. (In Portuguese).

Parashar, M., Wheeler, J. A., Pope G., Wang K., and Wang P., 1997. A New Generation EOS Compositional Reservoir Simulator: Part II – Framework and Multiprocessing, *paper SPE 37977, SPE Reservoir Simulation Symposium*, Dallas, USA, pp. 31-38.

Snir, M., Otto, S., Huss-Lederman, S., Walker, D., and Dongarra, J., 1996. *MPI: The complete reference*, Kowalik J. Editor, The MIT Press, London, England.

Stone, H. L., 1973, Estimation of Three-Phase Relative Permeability and Residual Data, *J. Can. Pet. Tech.*, vol. 12, 4, 53-61.

Thompson, J. F., Warsi, Z.U.A, and Mastin C. W., 1985. *Numerical Grid Generation – Foundations and Applications*, Elsevier Science Publishing, New York.

Wang, P., Yotov, I., Wheeler, M., Arbogast, T., Dawson, C., Parashar, M., and Sepehrnoori, K., 1997. A New Generation EOS Compositional Reservoir Simulator: Part I – Formulation and Discretization, *paper SPE 37079, SPE Reservoir Simulation Symposium*, Dallas, USA, pp. 55-64.